Phytomedicine Plus 3 (2023) 100447

Contents lists available at ScienceDirect

Phytomedicine Plus

journal homepage: www.sciencedirect.com/journal/phytomedicine-plus

In silico screening of phytochemicals from *Dissotis rotundifolia* against *Plasmodium falciparum* Dihydrofolate Reductase

Latif Adams [a], Michael Afiadenyo [b], Samuel Kojo Kwofie [c,d], Michael D. Wilson [b], Kwadow Asamoah Kusi [e], Dorcas Obiri-Yeboah [f], Siobhan Moane [a], Michelle McKeon-Bennett [a,*]

[a] *Technological University of Shannon: Midlands Midwest, Midlands campus, Athlone, Ireland*
[b] *Department of Parasitology, Noguchi Memorial Institute for Medical Research (NMIMR), College of Health Sciences (CHS), University of Ghana, Legon, Accra, Ghana*
[c] *Department of Biomedical Engineering, School of Engineering Sciences, College of Basic and Applied Sciences, University of Ghana, Legon, Accra, Ghana*
[d] *West African Center for Cell Biology and Infectious Pathogens, Department of Biochemistry, Cell and Molecular Biology, University of Ghana, Legon, Accra, Ghana*
[e] *Department of Immunology, Noguchi Memorial Institute for Medical Research (NMIMR), College of Health Sciences (CHS), University of Ghana, Legon, Accra, Ghana*
[f] *Department of Microbiology and Immunology, School of Medical Sciences, College of Health and Allied Sciences, University of Cape Coast, Cape Coast, Ghana*

ARTICLE INFO

Keywords:
Malaria
Antifolate
Dissotis rotundifolia
Phytochemical
Plasmodium falciparum Dihydrofolate Reductase (*Pf*DHFR)
Molecular docking
Molecular dynamics simulation

ABSTRACT

Background: Malaria remains a major health concern in developing countries with high morbidity and mortality, especially in pregnant women and infants. A major obstacle to the treatment of malaria is a low effectiveness and an increase resistance of the parasite to antimalarial drugs. As a result, there is an ongoing demand for new and potent antimalarial drugs. Medicinal plants remain a potential source for the development of new antimalarial drugs. Amongst them is *Dissotis rotundifolia* is an ethnomedical important plant used in West Africa to treat malaria.

Purpose: This study aimed at identifying new potential antifolates by virtually screening phytochemicals characterized from the whole plant methanolic extract of *D. rotundifolia* against *Plasmodium falciparum* Dihydrofolate Reductase (*Pf*DHFR).

Methods: LC-ESI-Q-TOF-MS analysis was employed to identify the phytochemicals present in the whole plant methanolic extract of *D. rotundifolia.* These phytochemicals were docked against the catalytic site of *Pf*DHFR. The docking protocol was evaluated using the Area Under the Curve (AUC) of a Receiver Operating Characteristic (ROC) curve. The binding mechanisms and the drug-likeness of the phytochemicals were characterized. A 100 ns Molecular Dynamics (MD) simulation and Molecular Mechanics-Poisson Boltzmann Surface Area (MM-PBSA) calculations were utilized to analyze the stability, the energy decomposition *per* residue and the binding free energy of the potential leads.

Results: Twenty nine phytochemicals were characterized and docked against *Pf*DHFR. Dimethylmatairesinol, flavodic acid, sakuranetin, and sesartemin were identified as potential leads with binding affinities of -8.4, -8.9, -8.6, and -8.9 kcal/mol respectively, greater than a stringent threshold of -8.0 kcal/mol. The potential leads also interacted hydrophobically with critical residue Phe58. A novel critical residue, Leu46 was identified to be crucial in the catalytic activity of *Pf*DHFR. The potential leads were also predicted to be anti-protozoal with a probability of active (Pa) value ranging from 0.319 to 0.537.

Conclusion: This study elucidates the potential inhibition of *Pf*DHFR by dimethylmatairesinol, flavodic acid, sakuranetin and sesartemin present in *D. rotundifolia.* These compounds are druglike, do not violate Lipinski's rule of five, have a high binding affinity to *Pf*DHFR, and interact with crucial residues involved in the catalytic activity *Pf*DHFR. Dimethylmatairesinol, flavodic acid, sakuranetin and sesartemin could therefore be further investigated and developed as new antifolate drugs for malaria.

* Corresponding author at: Technological University of Shannon: Midlands Midwest, Midlands Campus, University Road, Athlone, Co. Westmeath, Ireland.
E-mail address: michelle.mckeonbennett@tus.ie (M. McKeon-Bennett).

https://doi.org/10.1016/j.phyplu.2023.100447

Available online 1 April 2023

Abbreviations

ADMET	Absorption, Distribution, Metabolism, Excretion and Toxicity
dTMP	Deoxythymidine monophosphate
DHF	Dihydrofolate
dUMP	Deoxyuridine monophosphate
ITNs	Insecticide-Treated Bed Nets
LC-MS	Liquid Chromatography Mass Spectrometry
MM-PBSA	Molecular Mechanics-Poisson Boltzmann Surface Area
PASS	Prediction of Activity Spectra of Substances
*Pf*DHFR	*Plasmodium falciparum* Dihydrofolate Reductase
RMSD	Root Mean Square Deviation
RMSF	Root Mean Square Fluctuation
SMILES	Simplified Molecular Input Line Entry System
SP	Sulfadoxine-Pyrimethamine
THF	Tetrahydrofolate
WHO	World Health Organization

Introduction

Malaria is one of the leading causes of morbidity and mortality in children and pregnant women (Belete, 2020). According to the World Health Organization (WHO) Malaria Report, 241 million cases and 627, 000 deaths were recorded in 2020, with 80% of malaria fatalities occurring in children under 5 years old in Africa. Out of 33.8 million pregnancies recorded in 2020, 34% were exposed to malaria infection during pregnancy (WHO, 2021).

Malaria in pregnancy is associated with unfavorable outcomes such as maternal anemia, pre-term delivery, infant mortality, maternal death, stillbirth, abortion, and low birth weight (El Gaaloul et al., 2022). Studies have reported that 20% of all stillbirths in Africa are caused by malaria infection annually (Moore et al., 2017). According to WHO report, malaria in pregnancy resulted in approximately 819,900 newborns with low birthweight in Africa in 2020 (WHO, 2021).

WHO recommends the use of insecticide-treated bed nets (ITNs) and preventive treatment using Sulfadoxine-Pyrimethamine (SP) to control and prevent malaria in pregnancy (Anto et al., 2019). SP is administered during the second and third trimesters of pregnancy (Al Khaja and Sequeira, 2021). SP targets *Plasmodium* parasite dihydropteroate synthase and dihydrofolate reductase, by decreasing the amount of folic acid the malarial parasite needs to synthesize nucleic acids (Waller and Sampson, 2018). Intermittent preventive treatment with SP is very effective in decreasing the detrimental effects of malaria during pregnancy (Desai et al., 2015). However, these drugs have developed resistance and become less effective (Iwaloye et al., 2021). The emergence of these resistant strains poses a major challenge to malaria control and elimination, thus resulting in high morbidity and mortality of malaria (Dhorda et al., 2021), prompting the urgent need for the development of new and effective alternative antimalarial agents.

Over the years, antifolate malaria medications have targeted *Plasmodium falciparum* dihydrofolate reductase *(PfDHFR)* (Mharakurwa et al., 2011). Another major target of antimalarial medications is *PfDHFR)*-Thymidylate Synthase (*Pf*DHFR-TS), which is responsible for DNA synthesis. DHFR is linked metabolically to TS, (DHFR-TS) expressed as a bifunctional protein that plays a crucial role in the folate pathway (Heinberg and Kirkman, 2015; Shamshad et al., 2022).

DHFR-TS is made up of both the DHFR and the TS domains (Hyde, 2005). The TS domain converts deoxyuridine monophosphate (dUMP) to deoxythymidine monophosphate (dTMP), which undergoes further processes to result in DNA synthesis. The DHFR domain, on the other hand, converts dihydrofolate (DHF) to tetrahydrofolate (THF) which then leads to the production of N 5,10 – methylene-THF, which is a co-factor for the conversion of dUMP to dTMP by providing the methyl group required for this reaction (Figure S1) (Hadni et al., 2021; Iwaloye et al., 2021). Over the years, antifolate drugs were used to inhibit DHFR hence preventing the production of THF from DHF. This then stops the production of the methyl group needed to be used to produce dTMP, which is essential for DNA synthesis (Hadni and Elhallaoui, 2017; Mharakurwa et al., 2011). Pyrimethamine and cycloguanil are antifolates that have been used as antimalarial drugs (Henriquez and Williams, 2020).

DHF interacts with residues Ile14, Ala16, Trp48, Asp54, Phe58, Asn108, Leu164 and Thr185 in order to be reduced to THF. Ala16, Cys50, Ile51, Arg59, Asn108, and Leu164 have mutated leading to drug resistance (Hadni et al., 2021). All these mutated residues are situated in the active site of *Pf*DHFR. In general, the degree of resistance also increases with the number of mutations (Henriquez and Williams, 2020). Greater degrees of resistance were found in parasites with the Cys59Arg+Ser108Asn, Asn51Ile+Cys59Arg+Ser108Asn, Asn51Ile+Cys59Arg+Ser108Asn+Ile164Leu, and Cys59Arg+Ser108Asn+Ile 164Leu mutations, compared to parasites with only S108N mutation (Hadni et al., 2021; Kamchonwongpaisan et al., 2004). Ala16-Val+Ser108Thr, a different double mutant, is only connected to cycloguanil resistance. Since additional mutations could theoretically occur to undermine the new antifolates, concerns about the likelihood of developing new antifolates with extended beneficial treatment lifetimes are greatly heightened by this mutation-based resistance. The parasites' ability to mutate, however, is limited since they require a functioning DHFR (Kamchonwongpaisan et al., 2004). As a result, it might be conceivable to create inhibitors that are resistant to mutations and would also cause the *Pf*DHFR to stop functioning (Yuvaniyama et al., 2003).

Medicinal plants remain one of the potential sources for the development of new effective antimalarial drugs (Uzor et al., 2020). Two antimalarial drugs quinine and artemisinin were extracted and isolated from the bark of the *Cinchona officinalis* and *Artemisia annua* respectively (Ceravolo et al., 2021). According to WHO, about 80% of low and middle-level countries depend on medicinal plants for their primary healthcare needs (G. Bhat, 2022). These plants are generally easily accessible with fewer side effects as compared to orthodox drugs (Mohammadi et al., 2020) and serve as an alternative for the development of new therapeutic agents.

Dissotis rotundifolia (Sm) Triana is a medicinal plant that belongs to the family Melastomataceae. It is commonly referred to as a 'pink lady' and is widely distributed in tropical Africa. *D. rotundifolia* is used to treat several ailments and diseases such as diarrhea, cough, dysentery, conjunctivitis, bilharzia, peptic ulcer, stomachache, asthma, bronchitis, tuberculosis, venereal diseases and malaria (Yeboah and Osafo, 2017). Phytochemical investigation indicates that the whole plant is rich in C-glycosylflavones, namely, vitexin, isovitexin, orientin, and isoorientin (Rath et al., 2014). Pharmacological studies of this plant have demonstrated antibacterial (Abere et al., 2010), antiulcer (Adinortey et al., 2018), antioxidant (Adinortey et al., 2018), anti-diarrhoeal (Abere et al., 2010), anti-trypanosomal (Mann et al., 2009) and anti-plasmodial properties (Djehoue et al., 2020). The decoction of the leaves of D. rotundifolia is ethnomedicinally used in west Africa to treat malaria (Lagnika et al., 2016).

This study aimed at identifying new potential antifolates for malaria by virtually screening 29 phytochemicals characterized from a whole plant methanolic crude extract of *D. rotundifolia* against *Pf*DHFR using molecular docking analysis. The binding mechanism of the protein-ligand complexes were characterized. Molecular dynamics (MD) simulations and MolecularMechanics-Poisson Boltzmann Surface Area (MM-PBSA) calculations were also undertaken to provide insights into the binding mechanisms of *Pf*DHFR-ligand complexes.

Materials and methods

Liquid chromatography mass spectrometry (LC-MS) analysis

Sample preparation

The sample was prepared by measuring 1 mg of dried crude plant extract into 1 ml of methanol. The sample was further diluted in a 1:20 and filtered into an HPLC autosampler vial through a 0.22 μm PVDF membrane.

High-performance liquid chromatography coupled with electrospray ionization-quadrupole-time of flight-mass spectrometry

LC-ESI-Q-TOF-MS- qualitative analysis

Phytochemical profiling of bioactive compounds in *D. rotundifolia* whole plant methanolic extract were determined using an Agilent 6520 quadrupole time-of-flight mass spectrometer linked with Agilent 1200 HPLC system via dual ESI interface (Agilent Technologies, USA). A previously developed method was used for the characterization of phytochemicals with some modifications (Shukla et al., 2021). *D. rotundifolia* whole plant crude extract was separated using Agilent Poroshell 120 EC C18 column; 50 mm × 3 mm, 2.7 μm. The eluents were water with 0.1% formic acid (A) and acetonitrile (B). The gradient program was followed as 90% (B) for 25 min, then 90% (B) from 25 to 40 min, and then 10% (B) from 40 to 45 min, at a flow rate of 0.5 ml/min. The sample injection volume was 6 μl.

Agilent 6520 QTOF mass spectrometer with electrospray ionization in positive mode was used to conduct the qualitative analysis. As a nebulizing, collision, and drying gas, nitrogen was utilized. Nebulizer pressure, drying gas flow rate, and capillary temperature were all set to 40 psi, 12 l/min, and 350 °C, respectively. Compounds were identified using a mass range of *m/z* 50–1700 and a resolving power of at least 15,000 (FWHM). All of the Ion source's parameters, including Vcap, the fragmentor, the skimmer, and the octapole radio frequency peak voltage, were set to, respectively, 3500 V, 150 V, 65 V, and 750 V. Mass Hunter software version 10 (Agilent Technology) was used for data analysis.

Protein and compounds retrieval

The experimentally solved 3D structure of *Pf*DHFR-TS was retrieved from the Protein Data Bank (PDB ID 1J3K) (Burley et al., 2021). The structure was solved using the X-ray diffraction method and has a resolution of 2.10 Å. The protein is made up of two chains each of DHFR and TS (DHFR, chains A and C, and TS, chains B and D). The DHFR is complexed with WR99210 and NADP while TS is complexed with dUMP (Yuvaniyama et al., 2003). An integrated library composed of two antifolate malaria drugs, cycloguanil and pyrimethamine, a *Pf*DHFR inhibitor (WR99201), and 29 compounds characterized from methanol extract of *D. rotundifolia* whole plant were curated for this study.

Binding sites identification

Computed Atlas of Surface Topology of proteins (CASTp) (Tian et al., 2018) was employed to evaluate the binding pocket used for this study. The pocket was later analyzed in PyMOL version 2.5.0 (Yuan et al., 2017).

Protein and compounds preparation and virtual docking

The spatial data files (SDF) of the compounds were retrieved from PubChem (Sunghwan et al., 2021). The universal force field was used to minimize the energy of the compounds before they were later converted to Auto Dock files (pdbqt) using Open Babel (O'Boyle et al., 2011) integrated into PyRx version 0.8 (Dallakyan and Olson, 2015). The energy of the protein was minimized using the CHARM 27 all atoms force field by GROningen Machine for Chemical Simulation (GROMACS) version 2018 (Abraham et al., 2015). The energy minimization was to ensure stability during docking. The energy minimized protein and compounds were then subjected to molecular docking. To dock the 29 compounds against *Pf*DHFR, AutoDock Vina v.1.2.0 (Trott and Olson, 2009) was employed. Grid box dimensions of 30.1 Å, 32.9 Å and 39.4 Å centered at 41.1 Å, 51.4 Å and 49.8 Å all in the x, y, and z coordinates respectively utilized.

Validation of docking protocol

Pyrimethamine, chloroquine, sulfadoxine, WR99210, and cycloguanil were employed as the five potent inhibitors whose Simplified Molecular Input Line Entry System (SMILES) were used to create their decoys using the Database of Useful Decoys; Enhanced (DUD;E) (Mysinger et al., 2012). Along with those inhibitors, 350 decoys were created and docked using AutoDock Vina against *Pf*DHFR. The receiver operating characteristic (ROC) curve was created from the docking data, and the area under the curve (AUC) was calculated using the simple ROC version 1.3.1 (Goksuluk et al., 2016). AUC and ROC were generated using a non-parametric approach of curve fitting (DeLong et al., 2016) for SE estimation and CI as well as a Type I error of 0.05.

The ligand of the co-crystallized structure of *Pf*DHFR was removed and redocked. The co-crystallized ligand and the redocked ligand were aligned using the LigAlign algorithm (Heifets and Lilien, 2010) imbedded in PyMOl version 1.3 (Yuan et al., 2017). The Root Mean Square Deviation (RMSD) of the two ligands will then be calculated. The co-crystallized complex and the redocked complex were then superimposed in LigPlot+ version 1.4.5 (Laskowski and Swindells, 2011) to identify the common residues the ligand interacted with in both complexes. These approaches aid in accessing AutoDock Vina's ability to predict the binding pose.

Absorption, distribution, metabolism, excretion, and toxicity prediction

SwissADME is a web tool that estimates the physicochemical descriptors, pharmacokinetics properties, and ADME parameters of compounds (Daina et al., 2017). The SMILES of the compounds were utilized to evaluate the ADME parameters of the compounds. Lipinski's rule, Verber rule, Egan rule, Ghose filter, and Muegge rule were considered for the ADME parameters of the compounds. Toxicity profiling of the compounds was done with Osiris Datawarrior version 5.5.0 (Sander et al., 2015). Mutagenicity, tumorigenicity, irritability, and reproducible effectiveness were the parameters considered. All compounds that violated any of the ADMET protocols were eliminated.

Characterization of binding mechanism

To forecast the nature of interactions between the ligands and the protein, Ligplot+ version 1.4.5 (Laskowski and Swindells, 2011) was employed to generate 2D protein-ligand interactions. The top hit pose was preserved in "pdb" file format and then rendered in PyMOL version 2.5.0. The complexes were then used as inputs for Ligplot+ version.1.4.5. Green dashed lines represent hydrogen bonds and spoked arcs extending toward the ligands represent hydrophobic interactions. The interaction profiles were created using default parameters.

Biological activity prediction

Prediction of Activity Spectra of Substances (PASS) was used to predict the activity of the potential leads. PASS is a tool for assessing an organic drug-like molecule's overall bioactivity. Based on the structure of organic substances, PASS makes simultaneous predictions of numerous different forms of biological activity (Filimonov et al., 2014). The probability of active (Pa) and probability of inactive (Pi) values were generated to determine the level of the activities of the compounds.

An exhaustive search of the literature was also done to identify works done on the potential leads, their analogs, and derivatives against malaria.

Molecular dynamics simulation and molecular mechanics Poisson-Boltzmann surface area calculation

Molecular dynamics (MD) simulations were performed using GROMACS version 5.1.4. The four potential leads' complexes, the co-crystallized complex, the cycloguanil complex, and the unbound protein were subjected to a 100 ns MD simulation using the CHARMM27 all-atoms force field. The ligand topology was generated using SwissParam (Zoete et al., 2011). Before the simulation, the complexes and the protein were prepared by initially being solvated in a 1 nm cubic water box and later neutralized by adding ions. The energy of the complexes and the protein was minimized for relaxation to remove steric clashes or bad geometry. Equilibration of temperature (300 K) and density (1020 kg/m^3) was done for steps of 5000. The results of the simulation were then analyzed using root mean square deviation (RMSD), root mean square fluctuation (RMSF), and radius of gyration (Rg). The graphs were then generated via Xmgrace version 5.1.25.

To determine the free binding energy, Molecular Mechanics-Poisson Boltzmann Surface Area (MM-PBSA) calculations were performed using g_mmpbsa, a tool for high throughput MM-PBSA calculation (Kumari et al., 2014). For every 1 ns step throughout the 100 ns MD, the free energies of the complexes were calculated. The binding free energy contributions of the residues of *Pf*DHFR involved in the binding of each compound were also estimated *via* MM-PBSA calculations. The results were plotted using the R programming package (R Core, 2020).

Results and discussion

LC-MS analysis

In this present study, the phytochemical profiling of bioactive compounds from the methanol extract of *D. rotundifolia* whole plant were analyzed by LC-ESI-QTOF-MS. A total of 29 compounds belonging to different classes such as flavonoids, alkaloids, carboxylic acid, amino alcohol, quinoline, lignans, sesquiterpenoid, glycosides, terpenoids, lipid, hydroxycoumarin, phenols, azole, quinone, fatty acid, steroid, and quinoxaline were tentatively characterized from their mass data and MS spectra using Agilent LC-MS Qualitative Software (Mass Hunter) and Personal Compound Database and Library (PCDL). Additionally, the following public databases; Pubchem (Sunghwan et al., 2021), Chemspider (Pence and Williams, 2010), Phenol-Explorer (Rothwell et al., 2013), and Kegg Ligand Database (Kanehisa, 2002) were also used. The base peak chromatogram (BPC) of *D. rotundifolia* methanol crude extract in positive ionization mode is represented in Fig. 1.

Binding pocket identification

A binding site is a part of a protein that a ligand binds to with specificity (Stank et al., 2016). The binding pocket used for this work had a surface area of 755.741 Å^2 and a volume of 507.282 Å^3. This predicted pocket was chosen because it contained all the critical residues (Table S1) and is large enough to accommodate the ligands to fit through (Figure S2). Also, previous studies have shown that the mutations at this binding pocket are responsible for the resistance of *Pf*DHFR against drugs such as cycloguanil and pyrimethamine as they bind to this pocket (David et al., 2018; Hadni and Elhallaoui, 2017; Manhas et al., 2019). This is the site where DHF binds to be reduced to THF (Ibraheem et al., 2022; Yuvaniyama et al., 2003). In addition, this same pocket was used in previous studies, where potential *Pf*DHFR inhibitors were identified (Hadni et al., 2021; Iwaloye et al., 2021).

Validation of docking protocol

A ROC curve was generated after docking five *Pf*DHFR inhibitors and their decoys against the receptor to confirm AutoDock Vina's capability to differentiate between active and inactive molecules regarding the receptor (Fig. 2) (Enninful et al., 2022). To evaluate the docking performance, the AUC value was calculated. AUC values between 0.5 and 0.7 are regarded as moderate, larger than 0.7 as acceptable, and less than 0.5 as having poor discrimination ability. The docking model for the receptor has a great discriminating ability if the AUC value is very near 1 (DeLong et al., 2016). The AutoDock Vina system demonstrated good discriminatory capacity to distinguish between active compounds and decoys with an AUC of 0.733 a type I error of 0.05 and a p-value of 0.01216745.

The ligands of the co-crystallized structure and the redocked structure were aligned and an RMSD of 0.959 Å was obtained. According to (Alves et al., 2014), an RMSD less than or equal to 2.0 Å indicates a docking tool's ability to predict the pose of a ligand in a binding pocket (Fig. 3(A) and (B). The co-crystallized and the redocked complexes were later superimposed in LigPlot+. Out of the 11 residues that interacted with the ligand, 8 were common to both complexes. There were an overlapping of 2 hydrogen bonds with Asp54 and 5 hydrophobic interactions with Asn108, Phe58, Ile112, Cys54, and Pro113. Ile14 and Leu164 formed hydrophobic interactions with the ligand in the co-crystallized structure but in the redocked structure, formed hydrogen bonds (Fig. 3(C). This corroborates the results from the ligand alignment on AutoDock Vina's capability to determine the binding pose of ligands.

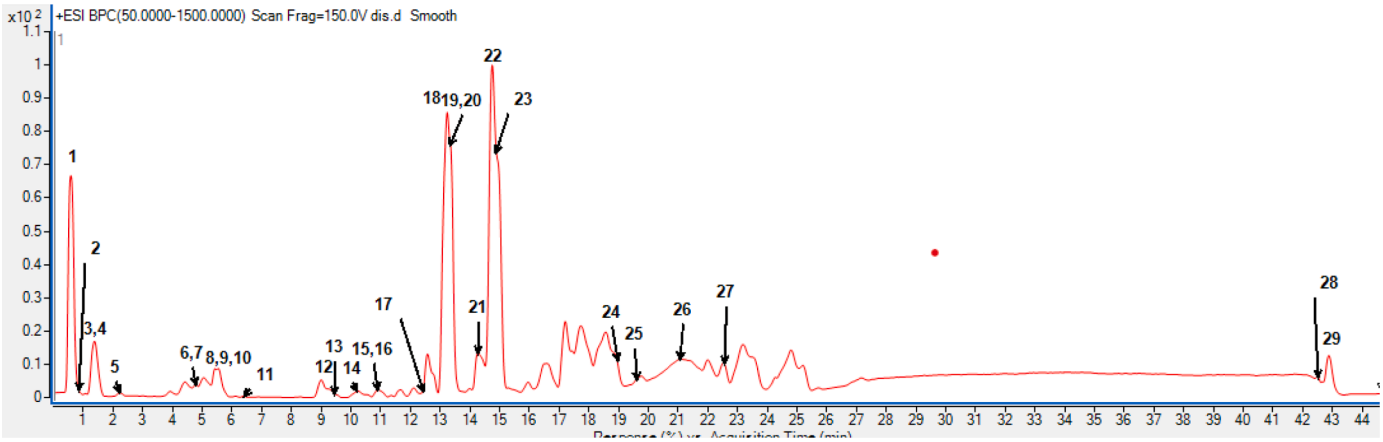

Fig. 1. The base peak chromatogram (BPC) of *Dissotis rotundifolia* whole plant methanol extract in positive ionization mode.

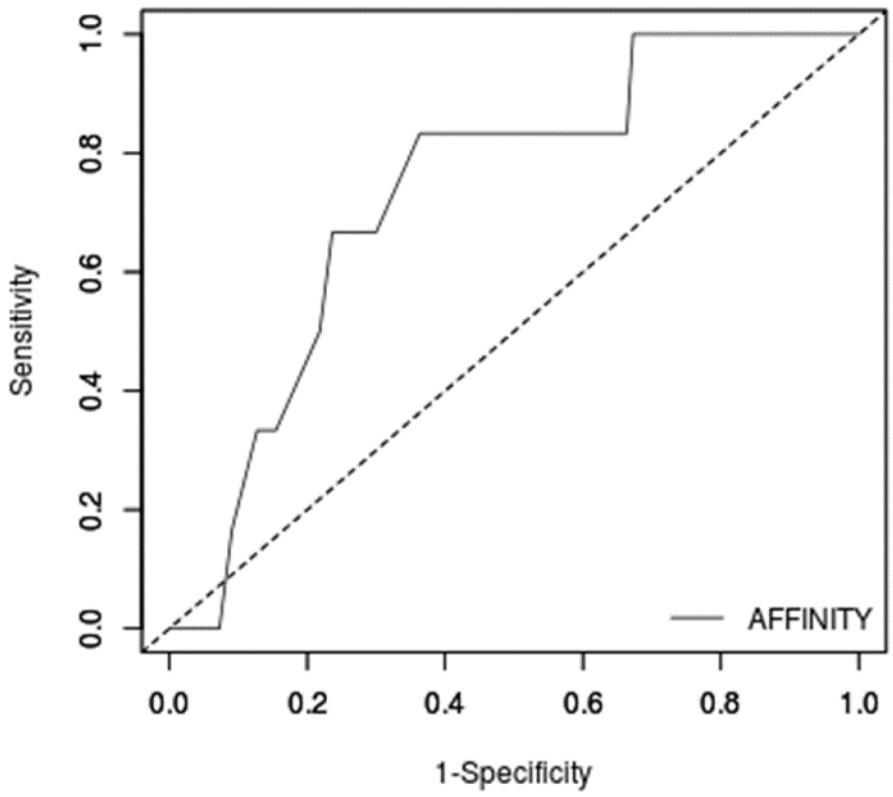

Fig. 2. The ROC curve generated via EasyROC to depict the capability of AutoDock Vina to differentiate between actives and inactives.

Molecular docking studies

Molecular docking primarily studies how two or more molecular structures fit together and the possible interaction existing between the structures (Stanzione et al., 2021). Using a scoring system, docking is utilized to assess the quality of the pose and predict the ligand shape, as well as its position and orientation within the protein binding site. The experimental binding mode should ideally be reproducible by the sampling process, and it should also be ranked top among all created poses by the scoring function (Stanzione et al., 2021). The 29 phytochemicals and 3 inhibitors were docked against the predicted binding pocket of *Pf*DHFR (Fig. 4). -7.0 kcal/mol is a good discriminating threshold for putative protein binders and non-binders (Chang et al., 2007). Inhibition is not necessarily improved by a more negative binding energy (Li et al., 2014; Pantsar and Poso, 2018). Because approximately 97.7% of inhibitors have binding energies of less than -7.0 kcal/mol (Chang et al., 2007), the threshold of -7.0 kcal/mol filters out approximately 95% of non-inhibitors (Ahmad et al., 2021). Furthermore, previous studies have shown that triclosan, an inhibitor of *Pv*DHFR (IC_{50} = 775 nM) and *Pf*DHFR (IC_{50} > 10 μM) has a binding affinity of -7.557 kcal/mol to *Pf*DHFR (Bilsland et al., 2018). As such, a stringent threshold of -8.0 kcal/mol was employed. All compounds with binding energies greater than -8.0 kcal/mol were not considered for further analysis. The compounds identified herein had lower binding energies (higher binding affinity) to *Pf*DHFR than cycloguanil and pyrimethamine, with binding energies of -8.0 kcal/mol and -7.6 kcal/mol, respectively. Out of the original 29 compounds, 15 had binding energies less than or equal to -8.0 kcal/mol and hence, were considered for downstream analysis (Table 1).

Absorption, distribution, metabolism, excretion, and toxicity (ADMET) evaluation

ADMET predictions were performed to remove compounds that may fail as drug candidates (Enninful et al., 2022). Lipinski's rule (Benet et al., 2016) determines whether a biologically active compound has the chemical and physical properties to be orally bioavailable (Benet et al., 2016). The number of hydrogen bond donors (≤ 5), hydrogen bond acceptors (≤ 10), water-octanol partition coefficient (log $P \leq 5$), and molecular weight (≤ 500) are the parameters considered to determine the bioavailability of a compound (Benet et al., 2016). Verber's rule (Veber et al., 2002) also predicts the bioavailability of drugs by considering the number of rotatable bonds (≤ 10) which is a measure of molecular flexibility (Khanna and Ranganathan, 2009) and the Topological Polar Surface Area (TPSA ≤ 140 $Å^2$) which is used to analyze the transport of a drug by multi resistance-associated proteins (Fernandes and Gattass, 2009). Ghose filter (Ghose et al., 1999), Egan rule (Egan et al., 2000), and Muegge rule (Muegge et al., 2001) also consider the molecular weight, TPSA, the number of rotatable bonds, hydrogen bonds donors and acceptors, log P and number of atoms to determine the bioavailability of a drug (Table 2). Toxicity testing is a requisite during drug discovery. Before clinical trials commence, the toxicity of a potential drug must be evaluated (Parasuraman, 2011). Out of the 15 compounds, 4 were suitable for further analysis (Table 3).

Characterization of protein-ligand interaction

The binding interactions of the hits were elucidated to evaluate the important intermolecular bonds involved in the complexes. CID1286 formed a hydrogen bond with Ala16 with a bond length of 3.11 Å and hydrophobic interactions with critical residues Phe58, Asp54, and Ile14. CID71944 formed 3 hydrogen bonds with three critical residues, Asp54, Thr185, and Ala16. CID73571 also formed 2 hydrogen bonds with Ala16. Both CID71944 and CID73571 formed hydrophobic interactions with Asn108, Cys15, Ser111, Leu40, Val195, Phe58 and Leu46. CID342737 on the other hand did not form a hydrogen bond but formed hydrophobic interactions with 15 residues (Fig. 5). WR99210 interacted hydrophobically with residues Ile14, Ala16, Cys15, Phe58, Ile112,

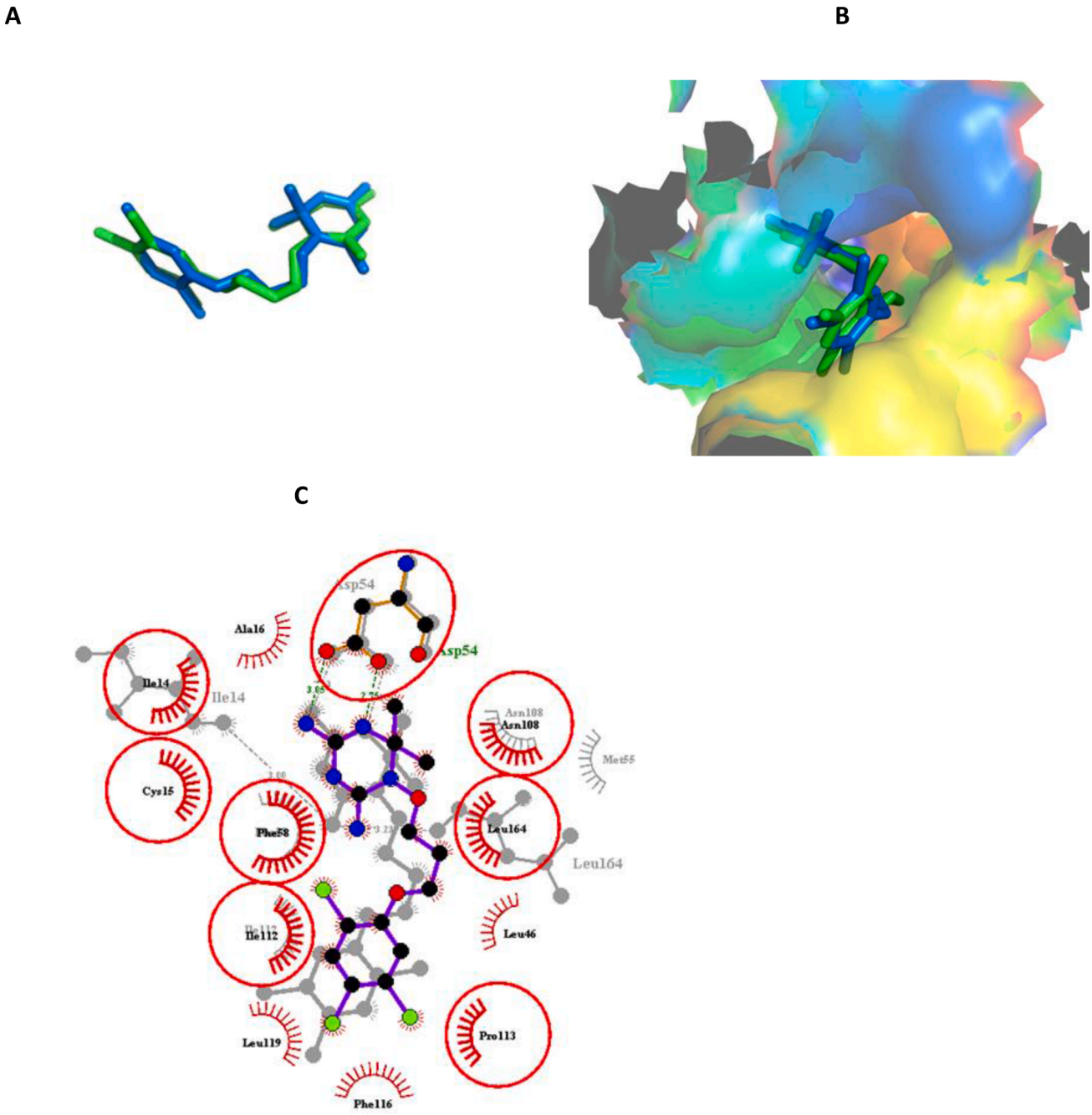

Fig. 3. Overlapping of the Ligands of the co-crystallized structure (green) and the redocked structure (blue) to determine the RMSD (A) and (B). The superimposition of the co-crystallized complex and the redocked complex (C).

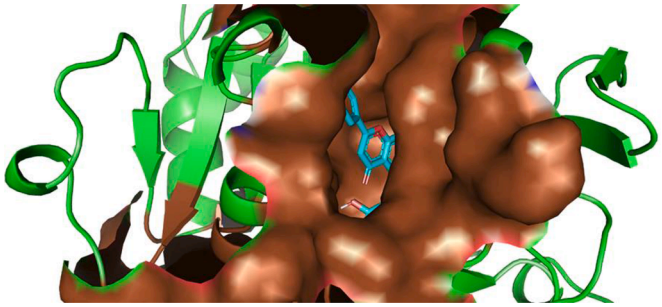

Fig. 4. CID71944 (blue) docked in the binding pocket (brown) of *Pf*DHFR with the rest of the protein shown as ribbon (green).

Leu119, Phe116, Pro113, Leu46, Leu164 and Asn108 while forming two hydrogen bonds with Asp54. Cycloguanil, on the other hand, formed a hydrogen bond with Asn108 and hydrophobic interactions with Phe58, Asp54, Ala16, Cys15, Leu164, Ile14, Tyr170, Leu40, and Leu46 (Figure S3). Interactions with residues Phe58 and Phe116 increase the anti-plasmodial action of naphyl derivatives carrying 1,2,3-triazole compounds significantly (Ibraheem et al., 2022). In addition, Phe58 is a critical residue involved in the catalytic activity of *Pf*DHFR, hence an interaction with Phe58 increases the plausibility of inhibition (Bilsland et al., 2018). Strong binding is indicated by the many hydrogen bonds and the small bond lengths, which could make these ligands intriguing compounds to further study (Enninful et al., 2022).

Table 1
Molecular docking results of the 29 phytochemicals and 4 antifolate drugs added as controls with their binding energies. Compounds with binding energy ≤ -8.0 kcal/mol were selected for further analysis.

	COMPOUND CID	BINDING ENERGY (kcal/mol)
1.	101,274,424	-9.8
2.	51,136,360	-9.7
3.	5,280,794	-9.7
4.	3,052,765	-9.5
5.	5,280,804	-9.3
6.	121,750 (WR99210)	-9.3
7.	12,309,350	-9.2
8.	85,260,329	-9.2
9.	162,350	-9
10.	71,944	-8.9
11.	342,737	-8.9
12.	73,571	-8.6
13.	46,173,908	-8.4
14.	1286	-8.4
15.	5,281,614	-8.3
16.	1530	-8.1
17.	9049 (Cycloguanil)	-8
18.	5,281,857	-7.9
19.	6,440,940	-7.8
20.	17,109	-7.7
21.	4993 (Pyrimethamine)	-7.6
22.	100,067	-7.6
23.	590,929	-7.2
24.	5,280,567	-7.1
25.	276,202	-6.8
26.	3610	-6.7
27.	1923	-6.5
28.	464	-6.4
29.	122,121	-6.2
30	8456	-6.2
31.	10,666	-5.9
32	69,421	-5.8
33.	37,511	-3.6

Prediction of biological activity

Biological activities with a probability of activity (Pa) > probability of inactivity (Pi) and Pa > 0.3, are considered potential compounds for those pharmacological activity investigations (Goel et al., 2010). In this study, we considered the antiprotozoal activity of the compounds since the malaria parasite belongs to the phylum protozoa (Dondorp and Von Seidlein, 2017). All the compounds were predicted as antiprotozoal activities with Pa ranging from 0.319 to 0.537 when Pa>Pi. The compounds CID324737, CID73571, CID71944, and CID1286 were predicted as possessing anti-protozoal activities with Pa values of 0.352, 0.476, 0.426, and 0.537 respectively (Table S4).

CID1286 is structurally similar to the natural compound (2R,3R)-taxifolin-3-O-α-L-rhamnoside, extracted from *Bafodeya benna* which has been shown to have antimalarial properties (Xu et al., 2011). Kaempferol-3-*O*-rhamnoside, which is also an analog of CID1286 has been proven to possess antimalarial activity (Barliana et al., 2014). CID71944 has similar side chains as ethylenediamine-N,N'-diacetic acid, an iron-chelating drug that was given to rats injected with *P. berghei,* and antimalarial activity was observed. Ethylenediamine-N,N'-diacetic acid was later tested on human red blood cells infected with *P. falciparum* cultures and antiplasmodial activity was observed (Yinnon et al., 1989). CID73571 which is structurally similar to a naringenin derivative isovitexin-(I-3,II-3)-naringenin has been identified to possess antiplasmodial activity (Xu et al., 2011). CID342737 is a benzodioxole and studies (Nelson and Hoosseintehrani, 1982) has shown that benzodioxole natural compounds possess antimalarial properties.

Molecular dynamics simulations

The protein-ligand complexes and the unbound protein were subjected to 100 ns MD simulations. RMSD, RMSF, and Rg analysis were performed on the MD outputs of all the systems and the graphs were generated. To evaluate the stability of the complexes, the RMSD graph was analyzed.

The RMSD is used to measure the displacement of the atoms from the backbone (Raschka, 2017). The main application of RMSD is to compare the differences between the structures that were present during the simulation period and their reference structure. The RMSD trajectory displays the time-dependent difference between a protein structure and

Table 3
The toxicity profiling results generated with OSIRIS DataWarrior. Compounds predicted to be toxic in at least one of the parameters were excluded from the downstream analysis.

Compound CID	Mutagenic	Reproductive effect	Tumorigenic	Irritant
101,274,424	None	None	High	None
51,136,360	None	None	None	None
5,280,794	None	None	None	None
3,052,765	None	None	High	None
1530	High	High	High	None
5,281,614	High	None	None	None
162,350	None	None	None	None
12,309,350	None	None	None	None
46,173,908	None	None	None	High
52,800,804	None	None	None	None
85,260,329	High	None	Low	None
1286	None	None	None	None
71,944	None	None	None	None
73,571	None	None	None	None
324,737	None	None	None	None

Table 2
ADME results generated by SwissADME showing the compounds that violated the various druglikenesss rules of the potential leads.

Compound CID	Number of violations Lipinski's rule of five	Veber rule	Egan rule	Ghose rule	Muegge rule	GI absorption
342,737	0	0	0	0	0	High
71,944	0	0	2	0	0	High
73,571	0	0	0	0	0	High
1286	0	0	0	0	0	High
1530	0	0	0	0	0	High
5,281,614	0	0	0	0	0	High
162,350	1	0	1	1	2	Low
12,309,350	2	0	1	1	3	Low
101,274,424	0	1	1	0	1	Low
51,136,360	2	1	1	0	3	Low
5,280,794	1	0	1	3	2	Low
3,052,765	0	0	0	0	0	High
46,173,908	3	2	1	4	5	Low
52,800,804	2	1	1	1	3	Low
85,260,329	2	1	1	1	4	Low

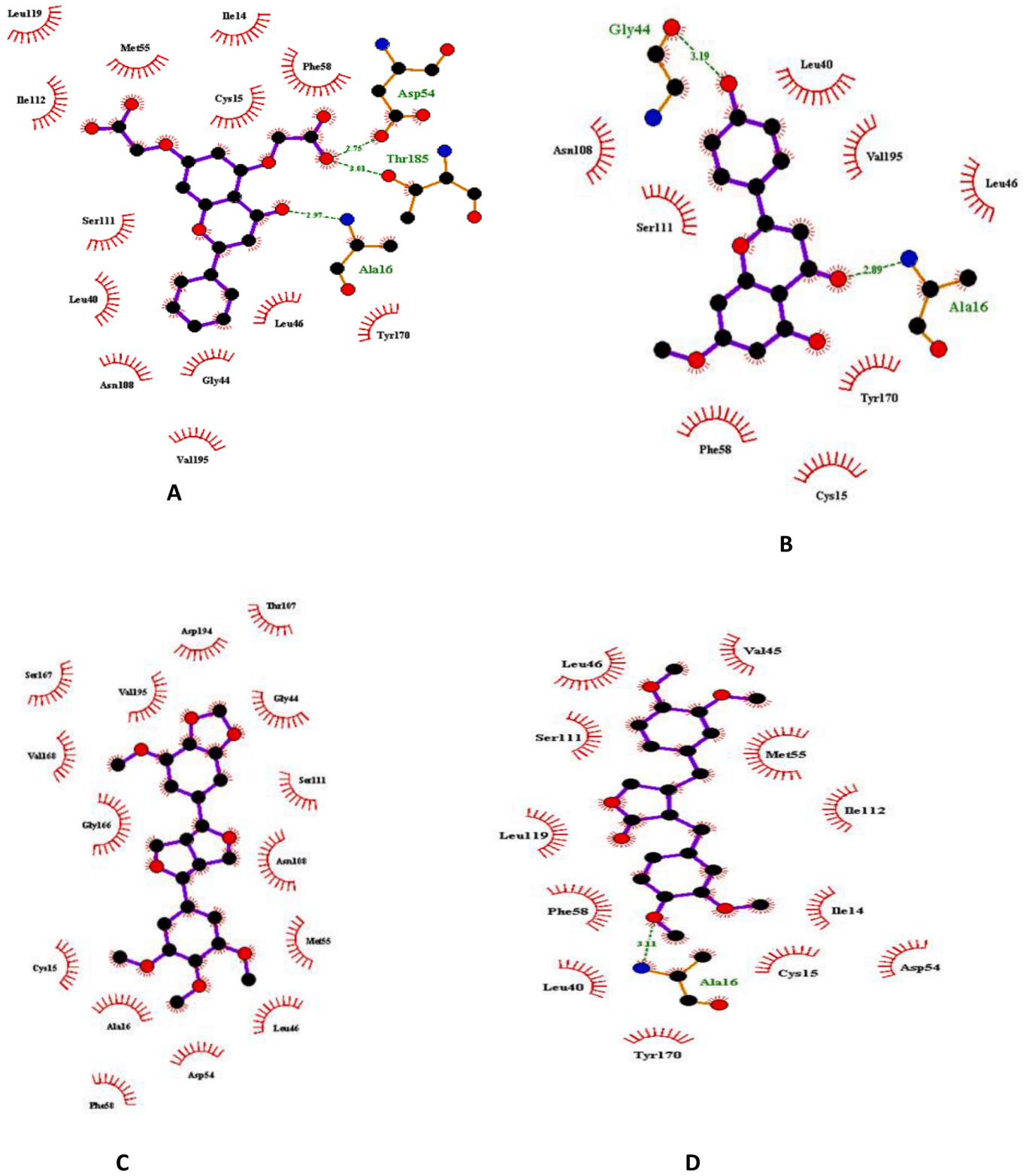

Fig. 5. Protein-ligand interaction of (A) *Pf*DHFR-CID 71,944, (B) *Pf*DHFR-CID1286, (C) *Pf*DHFR-CID73571, and (D) *Pf*DHFR-CID342737 complexes. The green dash indicates hydrogen.

its reference structure (Enninful et al., 2022). All the complexes and the unbound protein RMSD rose from 0 ns to about 0.225 nm until stability was reached. The co-crystallized complexed (DHFR-WR99210) rose from 0 to 0.3 nm. From 10 to 20 ns, a high fluctuation was observed for the DHFR-WR99210 complex. This depicts a higher displacement of the atoms from the backbone. Form 20 to 50 ns, stable fluctuations with an average of ~0.23 nm. About 0.125 nm displacement was observed between the unbound protein and DHFR-WR99210 complex around 60 ns. From 60 ns to the end of the simulation time, an average RMSD value of ~0.23 nm was observed. The DHFR-cycloguanil complex was stable throughout the simulation time with an average RMSD of ~0.2 nm. This observation was not observed in the DHFR-WR99210 complex. This

might be due to the WR99210 causing a serious clash with Asn108 (Yuvaniyama et al., 2003). Throughout the simulation time, the DHFR-CID1286 complex was steady with an average of 0.25 nm similar to that of the unbound protein but fluctuated around 14, 25, and 50 ns. DHFR-CID1286 was the complex with RMSD closer to the DHFR-WR99210. DHFR-CID71944 complex dropped from 0.225 nm to 0.175 nm around 8 ns then rose back to 0.225 nm around 20 ns. It then dropped back to 0.175 nm around 30 ns and stabilized throughout the simulation time with an average RMSD of 0.2 nm while fluctuating around 60 ns. DHFR-CID73571 fluctuates until around 30 ns and then stabilized with an RMSD of ~0.225 nm. DHFR-CID342737 had the highest RMSD apart from the DHFR-WR99210 complex, with an average of 0.225 nm until 40 ns then 0.25 nm from 40 ns to the end of the simulation time (Fig. 6).

Rg is used to evaluate the compactness of proteins (Jiang et al., 2019). A protein that is folded consistently will probably keep Rg at a very constant value (Lobanov et al., 2008). A protein's Rg will evolve if it unfolds (Enninful et al., 2022). DHFR-WR2210 complex was stabilized with an average Rg of ~1.85 nm. DHFR-cycloguanil had an average Rg of ~1.83 nm. In comparison to the co-crystallized and cycloguanil complexes, the potential leads complexes are stable indicating the folding of the potential lead complexes. Rg of DHFR-CID71944 stabilized throughout the simulation time. DHFR-CID1286 and DHFR-CID73571 behaved similarly. From 80 ns, the Rg of both complexes dropped but that of DHFR-CID73571 averaged around 1.86 nm, and that of DHFR-CID1286 with an average of 1.82 nm. DHFR-CID342737 stabilized till 20 ns, then fluctuated until 40 ns where a rise was observed. Stability was observed until 70 ns where a sharp rise to 1.89 nm was observed, then dropped to 1.84 nm around 85 ns. From 90 to 100 ns, a stable fluctuation was observed (Fig. 7).

To determine which DHFR residues are responsible for the structural variations, the RMSF trajectories of the DHFR-ligand complexes were also assessed. RMSF is connected to crystallographic B-factors and is used to assess the flexibility of various protein regions (Sinha and Wang, 2020). These protein domains are crucial in catalysis and ligand binding, and higher RMSF values indicate larger volatility (Dong et al., 2018). All the complexes behaved similarly throughout the simulation time. Higher fluctuations were observed in DHFR-WR99210 around residue 25 with an RMSF of 0.41 nm, DHFR-CID73571 around residue 45 with an RMSF around 0.3 nm, DHFR-CID71944 from residues 80 to 100 with an RMSF around 0.25 nm,DHFR-CID1286 around residue 130 with an RMSF 0.45 nm and DHFR-CID342737 around residue 190 with an RMSF of 0.15 nm. DHFR-cycloguanil and DHFR-CID71944 complexes fluctuated with an RMSF of 0.35 nm at residue 231 (Fig. 8).

Molecular Mechanics- Poisson Boltzmann surface area (MM-PBSA) calculation

The estimations of the protein-ligand binding affinities produced by simulation-based techniques like MM-PBSA are more accurate than those produced by other computational techniques like docking. By examining the binding free energy of protein-ligand complexes, it is possible to determine which ligands have higher binding affinities to the target. (Wang et al., 2017).

The binding free energies of the DHFR-CID324737 complex were the lowest (-84.648 kJ/mol) and corresponded with the docking score of -8.9 kcal/mol. This indicates that the DHFR-CID324737 complex had the highest binding affinity irrespective of the fact that no hydrogen bond was formed. DHFR-CID1286, DHFR-CID71944, and DHFR-CID73571 had free binding energies of -82.062, -51.988, and 60.157 kJ/mol with docking scores of -8.4, -8.9 and -8.6 kcal/mol, respectively. All the complexes had van der Waals forces ranging from -152.495 to -114.345 kJ/mol. DHFR-WR99210 complex (redocked complex) had binding energy of -9.3 kcal/mol after docking but had a binding free energy of -81.474 kJ/mol. DHFR-cycloguanil complexes had a binding energy of -8.0 kcal/mol and a free binding energy of -54.287 kJ/mol. This corroborates the docking results where all the potential leads had binding affinity greater than the DHFR-cycloguanil complex. This indicates that the potential leads have a higher chance of inhibiting *Pf*DHFR. DHFR-WR99210 complex had a higher binding affinity than all

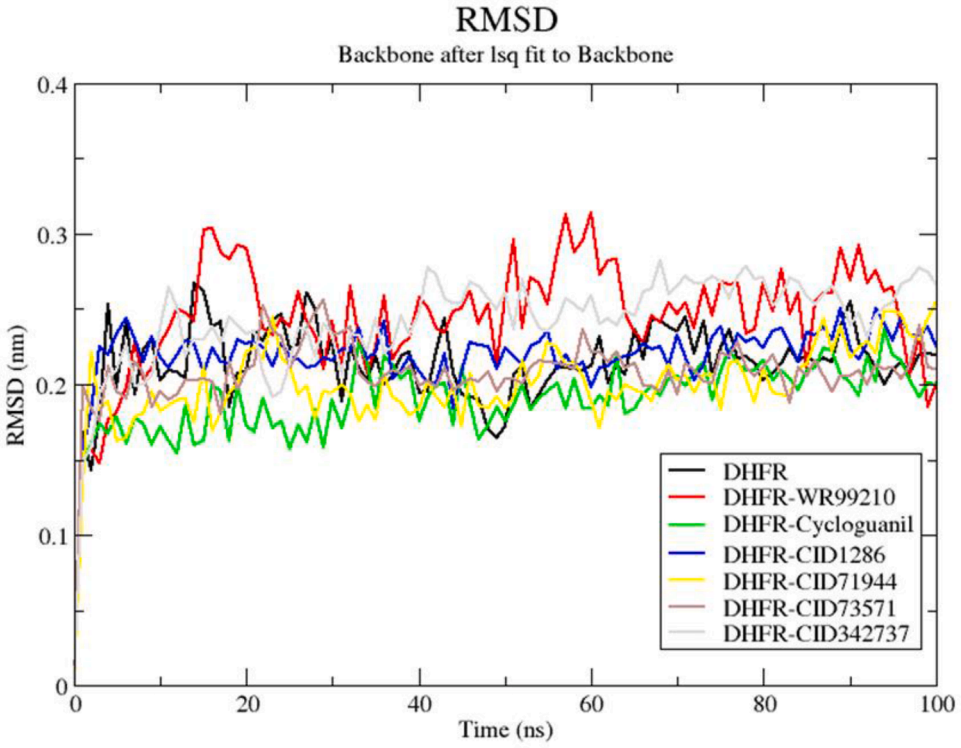

Fig. 6. The RMSD plot of the unbound protein (black) and the DHFR-ligand complexes after the 100 ns MD simulation. RMSD plots of DHFR-WR99210, DHFR-Cycloguanil, DHFR-CID1286, DHFR-CID71944, and DHFR-CID73571 DHFR-CID342737, are shown in red, green, blue, yellow, brown and gray respectively.

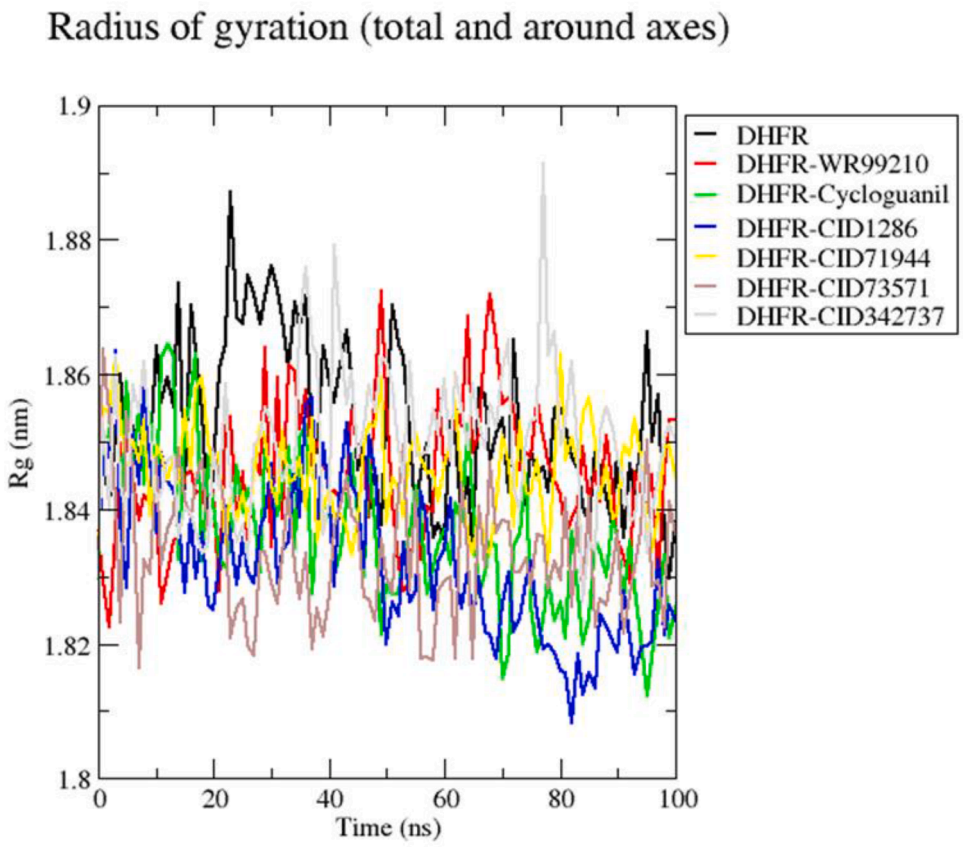

Fig. 7. Radius of Gyration plots of the unbound *Pf*DHFR (black) and the *Pf*DHFR-ligand complexes after the 100 ns MD. Rg plots of DHFR-WR99210, DHFR-Cycloguanil, DHFR-CID1286, DHFR-CID71944, and DHFR-CID73571 DHFR-CID342737, are shown in red, green, blue, yellow, brown and gray respectively.

the potential leads but from the MM-PBSA calculations, CID1286 and CID342737 had higher binding affinities than thaWR99210. Since it has been shown that binding energy from simulations is more accurate than computational docking, CID1286 and CID342737 have higher binding affinity to *Pf*DHFR than WR99210. (Table 4). A higher binding affinity indicates the plausibility of inhibition (Cunha et al., 2016). According to previous studies, the binding energy is mostly influenced by electrostatic and van der Waal's forces (Deng et al., 2011).

Energy decomposition per residue can be evaluated using MM-PBSA. This entails the breakdown of each residue by taking into account the interactions that each residue is a part of (Gupta et al., 2018). Considered crucial for protein-ligand binding are residues that contribute energies larger than or equal to 5 kJ/mol or less than or equal to -5 kJ/mol (Dankwa et al., 2022). In the DHFR-WR99210 complex, Asp54 contributed 16.63 kJ/mol, and Phe58 contributed -8.10 kJ/mol (Figure S5). Asp54 contributed 10.67 kJ/mol and Phe58 contributed -4.92 kJ/mol in the DHFR-cycloguanil complex (Figure S6). Leu46 contributed -7.32, -5.65, -4.76, and -6.87 kJ/mol in CID1286 (Fig. 9), CID71944, CID73571 and CID342737 complexes' respectively. This indicates that Leu46 may be a critical residue in the activity of *Pf*DHFR. From previous studies, Asp54 is a critical residue in the catalytic activity of *Pf*DHFR (Singh and Mishra, 2018), this is validated by the results obtained where among all the complexes, Asp54 contributed the highest energy.

Conclusion

Out of 29 bioactive compounds screened against *Pf*DHFR, four potential leads, dimethylmatairesinol, flavodic acid, sakuranetin, and sesartemin were identified as potential antifolates after molecular docking. ADMET analysis shows that all the potential leads do not violate Lipinski's rule, Verber rule, Egan rule, Muegge rule, and Ghose rule. All the potential leads also have high gastrointestinal absorption and were predicted not to be toxic.

These compounds have been predicted to be good binders of *Pf*DHFR by having high binding affinities (-8.4, -8.9, -8.6, and -8.9 kcal/mol, respectively) and interact with the critical residues involved in the activity of *Pf*DHFR in converting DHF to THF. In addition, MD simulation was carried out on the protein-ligand complexes to elucidate the conformational changes of the complexes and the unbound protein. MM-PBSA calculations identified novel critical residue Leu46, contributing a lot of energy to the catalytic activity of *Pf*DHFR. This depicts the stability of the protein-ligand complexes. These compounds can therefore be experimentally investigated by in vitro and in vivo techniques to determine their potential efficacy against *P. falciparum* strains and thus be developed into new antifolate drugs for malaria.

Funding

This study was supported by the TUS President's Doctoral Fellowship, grant number PA01034, the HEA [Higher Education Authority] and DFHERIS [The Department of Further and Higher Education, Research, Innovation, and Science, Ireland].

Availability of data and materials

All data generated and analyzed during this study are included in this manuscript and the supplementary data

CRediT authorship contribution statement

Latif Adams: Conceptualization, Investigation, Methodology,

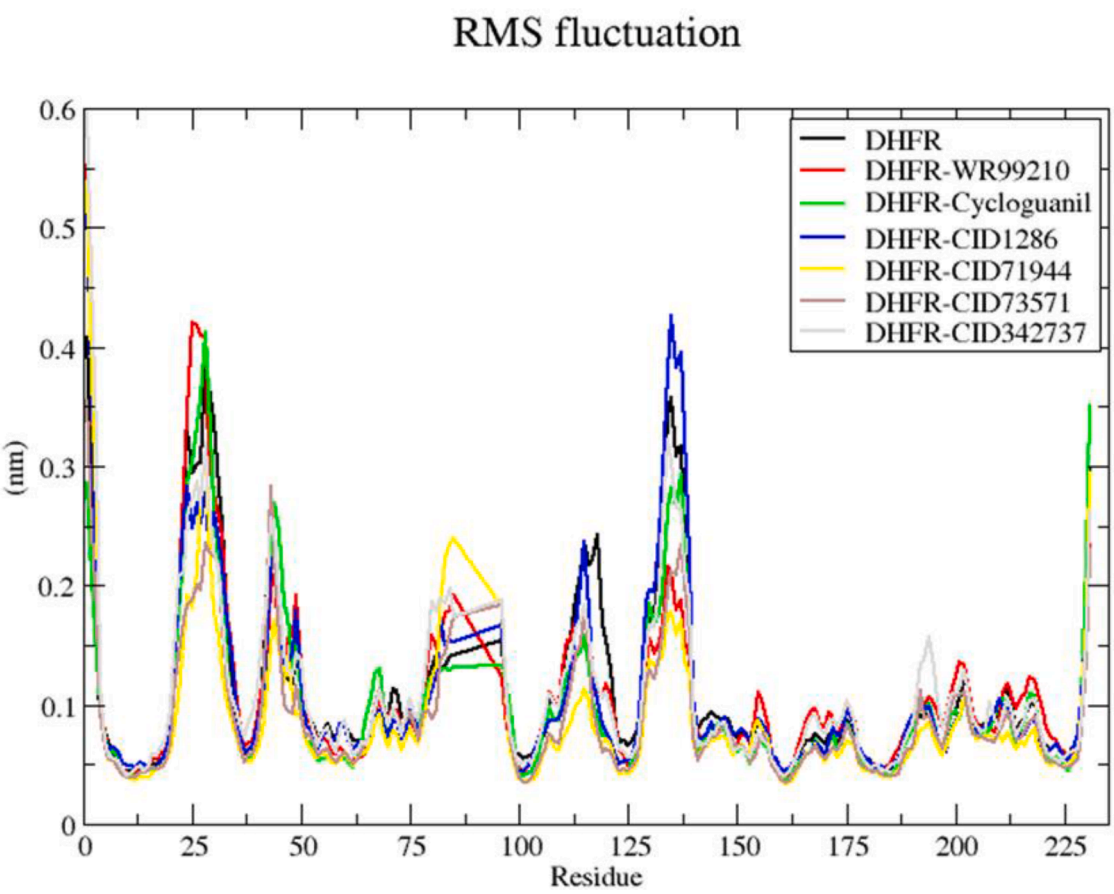

Fig. 8. RMSF of the unbound *Pf*DHFR protein (black) and the *Pf*DHFR-ligand complexes. The RMSF plots of DHFR-WR99210, DHFR-Cycloguanil, DHFR-CID1286, DHFR-CID71944, and DHFR-CID73571 DHFR-CID342737, are shown in red, green, blue, yellow, brown and gray respectively.

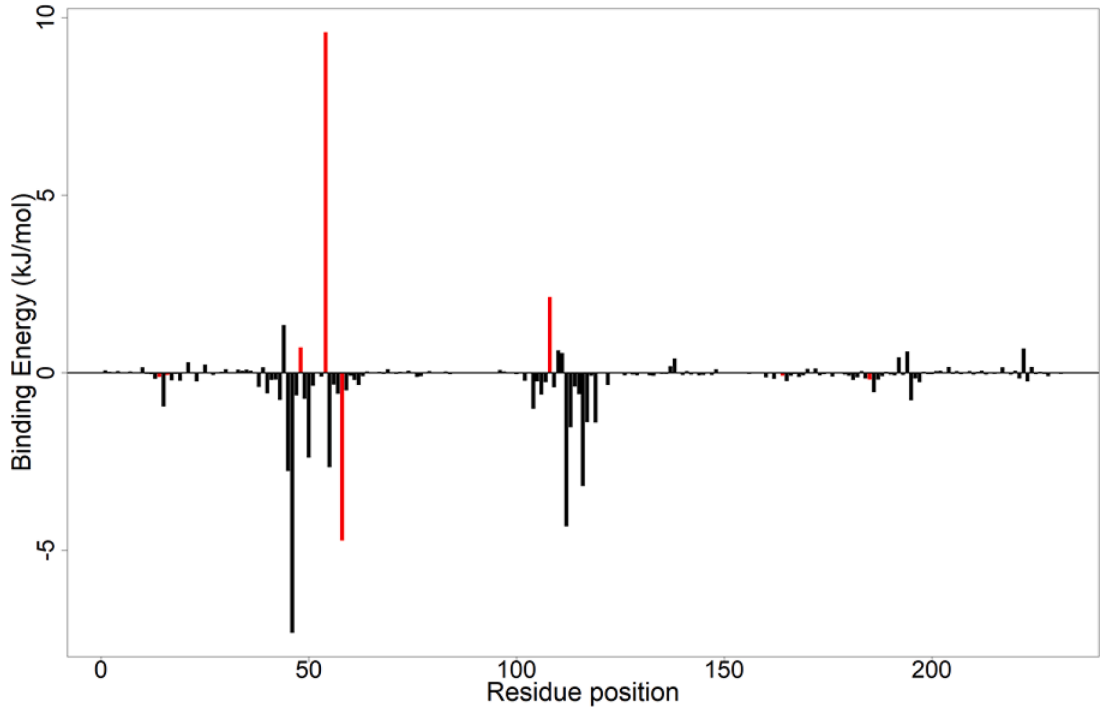

Fig. 9. Energy contribution of the *Pf*DHFR residues involved in the binding in the *Pf*DHFR-CID1286 complex.

Table 4
Binding free energies and the other contributing energies of the DHFR-ligand complexes from MM-PBSA computation Energy values are presented as average standard deviations in kJ/mol.

Compound	van der Waals Forces (kJ/mol)	Electrostatic Energy (kJ/mol)	Polar Solvation Energy (kJ/mol)	SASA (kJ/mol)	Binding Energy (kJ/mol)
CID1286	-152.495 ± 59.518	-19.914 ± 14.769	107.552 ± 50.624	-17.205 ± 6.846	-82.062 ± 41.853
CID342737	-155.890 ± 71.250	-25.130 ± 15.249	114.059 ± 50.339	-17.687 ± 7.716	-84.648 ± 64.468
CID71944	-129.803 ± 19.879	-53.621 ± 20.936	149.483 ± 31.000	-18.058 ± 2.423	-51.998 ± 16.282
CID73571	-114.345 ± 62.608	-24.015 ± 17.403	90.103 ± 60.616	-11.800 ± 6.444	-60.157 ± 44.055
WR99210	-144.231 ± 30.563	-9.186 ± 11.530	88.628 ± 26.888	-16.684 ± 3.242	-81.474 ± 27.398
Cycloguanil	-74.333 ± 53.490	-11.750 ± 14.079	40.638 ± 60.257	-8.842 ± 60.174	-54.287 ± 38.308

Project administration, Writing – original draft. **Michael Afiadenyo:** Data curation, Formal analysis, Writing – original draft. **Samuel Kojo Kwofie:** Data curation, Formal analysis, Writing – original draft. **Michael D. Wilson:** Data curation, Formal analysis. **Kwadow Asamoah Kusi:** Investigation, Methodology, Writing – review & editing. **Dorcas Obiri-Yeboah:** Supervision, Writing – review & editing. **Siobhan Moane:** Investigation, Methodology, Supervision, Writing – review & editing. **Michelle McKeon-Bennett:** Conceptualization, Funding acquisition, Project administration, Supervision, Writing – review & editing.

Declaration of Competing Interest

The authors declare that they have no known competing financial interests or personal relationships that could have appeared to influence the work reported in this paper.

Acknowledgments

The high-performance computing systems used for biocomputing known as Zuputo is located at the WACCBIP, University of Ghana.

Supplementary materials

Supplementary material associated with this article can be found, in the online version, at doi:10.1016/j.phyplu.2023.100447.

References

Abere, T.A., Okoto, P.E., Agoreyo, F.O., 2010. Antidiarrhoea and toxicological evaluation of the leaf extract of *Dissotis rotundifolia* triana (Melastomataceae). BMC Complement. Altern. Med. 10, 71. https://doi.org/10.1186/1472-6882-10-71.

Abraham, M.J., Murtola, T., Schulz, R., Páll, S., Smith, J.C., Hess, B., Lindahl, E., 2015. GROMACS: high performance molecular simulations through multi-level parallelism from laptops to supercomputers. SoftwareX 1–2, 19–25. https://doi.org/10.1016/j.softx.2015.06.001.

Adinortey, M., Ansah, C., Adinortey, C., McGiboney, J., Nyarko, A., Inhibition, vitro H + /K + -ATPase, 2018. Antiradical effects of a flavonoid-rich fraction of *Dissotis rotundifolia,* and In silico PASS Prediction of its isolated compounds. J. Nat. Sci. Biol. Med. 9, 47. https://doi.org/10.4103/jnsbm.JNSBM_104_17.

Ahmad, S., Waheed, Y., Abro, A., Abbasi, S.W., Ismail, S., 2021. Molecular screening of glycyrrhizin-based inhibitors against ACE2 host receptor of SARS-CoV-2. J. Mol. Model. 27, 206. https://doi.org/10.1007/s00894-021-04816-y.

Al Khaja, K.A.J., Sequeira, R.P., 2021. Drug treatment and prevention of malaria in pregnancy: a critical review of the guidelines. Malar. J. 20, 1–13. https://doi.org/10.1186/S12936-020-03565-2/TABLES/3.

Alves, M.J., Froufe, H.J.C., Costa, A.F.T., Santos, A.F., Oliveira, L.G., Osório, S.R.M., Abreu, R.M.V., Pintado, M., Ferreira, I.C.F.R., 2014. Docking studies in target proteins involved in antibacterial action mechanisms: extending the knowledge on standard antibiotics to antimicrobial mushroom compounds. Molecules 19, 1672–1684. https://doi.org/10.3390/molecules19021672.

Anto, F., Agongo, I.H., Asoala, V., Awini, E., Oduro, A.R., 2019. Intermittent preventive treatment of malaria in pregnancy: assessment of the sulfadoxine-pyrimethamine three-dose policy on birth outcomes in rural northern Ghana. J. Trop. Med. 2019, 1–10. https://doi.org/10.1155/2019/6712685.

Barliana, M.I., Suradji, E.W., Abdulah, R., Diantini, A., Hatabu, T., Nakajima-Shimada, J., Subarnas, A., Koyama, H., 2014. Antiplasmodial properties of kaempferol-3-O-rhamnoside isolated from the leaves of Schima wallichii against chloroquine-resistant *Plasmodium falciparum*. Biomed. Reports 2, 579–583. https://doi.org/10.3892/br.2014.271.

Belete, T.M., 2020. Recent progress in the development of new antimalarial drugs with novel targets. Drug Des. Devel. Ther. 14, 3875–3889. https://doi.org/10.2147/DDDT.S265602.

Benet, L.Z., Hosey, C.M., Ursu, O., Oprea, T.I., 2016. BDDCS, the Rule of 5 and drugability. Adv. Drug Deliv. Rev. https://doi.org/10.1016/j.addr.2016.05.007.

Bilsland, E., Van Vliet, L., Williams, K., Feltham, J., Carrasco, M.P., Fotoran, W.L., Cubillos, E.F.G., Wunderlich, G., Grøtli, M., Hollfelder, F., Jackson, V., King, R.D., Oliver, S.G., 2018. *Plasmodium* dihydrofolate reductase is a second enzyme target for the antimalarial action of triclosan. Sci. Rep. 8, 1–8. https://doi.org/10.1038/s41598-018-19549-x.

Burley, S., Bhikadiya, C., Bi, C., Bittrich, S., Chen, L., Crichlow, G.V., Christie, C.H., Dalenberg, K., Di Costanzo, L., Duarte, J.M., Dutta, S., Feng, Z., Ganesan, S., Goodsell, D.S., Ghosh, S., Green, R.K., Guranović, V., Guzenko, D., Hudson, B.P., Lawson, C.L., Liang, Y., Lowe, R., Namkoong, H., Peisach, E., Persikova, I., Randle, C., Rose, A., Rose, Y., Sali, A., Segura, J., Sekharan, M., Shao, C., Tao, Y.-P., Voigt, M., Westbrook, J.D., Young, J.Y., Zardecki, C., Zhuravleva, M., 2021. RCSB Protein Data Bank: powerful new tools for exploring 3D structures of biological macromolecules for basic and applied research and education in fundamental biology, biomedicine, biotechnology, bioengineering and energy sciences. Nucleic Acids Res. 49, D437–D451. https://doi.org/10.1093/nar/gkaa1038.

Ceravolo, I.P., Aguiar, A.C., Adebayo, J.O., Krettli, A.U., 2021. Studies on activities and chemical characterization of medicinal plants in search for new antimalarials: a ten year review on ethnopharmacology. Front. Pharmacol. 12, 2478. https://doi.org/10.3389/fphar.2021.734263/.

Chang, M.W., Lindstrom, W., Olson, A.J., Belew, R.K., 2007. Analysis of HIV wild-type and mutant structures via in silico docking against diverse ligand libraries. J. Chem. Inf. Model. 47, 1258–1262. https://doi.org/10.1021/ci700044s.

Cunha, N., Teixeira, G., Martins, T., Souza, A., Oliveira, P., Símaro, G., Rezende, K., Gonçalves, N., Souza, D., Tavares, D., Silva, M., dos Santos, R., 2016. (−)-Hinokinin induces G2/M arrest and contributes to the antiproliferative effects of doxorubicin in breast cancer cells. Planta Med. 82, 530–538. https://doi.org/10.1055/s-0042-101761.

Daina, A., Michielin, O., Zoete, V., 2017. SwissADME: a free web tool to evaluate pharmacokinetics, drug-likeness and medicinal chemistry friendliness of small molecules. Sci. Rep. 7, 1–13. https://doi.org/10.1038/srep42717.

Dallakyan, S., Olson, A.J., 2015. Small-molecule library screening by docking with PyRx. Methods in Molecular Biology (Clifton, N.J.), pp. 243–250. https://doi.org/10.1007/978-1-4939-2269-7_19.

Dankwa, B., Broni, E., Enninful, K.S., Kwofie, S.K., Wilson, M.D., 2022. Consensus docking and MM-PBSA computations identify putative furin protease inhibitors for developing potential therapeutics against COVID-19. Struct. Chem. https://doi.org/10.1007/s11224-022-02056-1.

David, T.I., Adelakun, N.S., Omotuyi, O.I., Metibemu, D.S., Ekun, O.E., Eniafe, G.O., Inyang, O.K., Adewumi, B., Enejoh, O.A., Owolabi, R.T., Oribamise, E.I., 2018. Molecular docking analysis of phyto-constituents from Cannabis sativa with pfDHFR. Bioinformation 14, 574–579. https://doi.org/10.6026/97320630014574.

DeLong, E.R., Delong, D.M., Clarke-Pearson, D.L., 2016. Comparing the areas under two or more correlated receiver operating characteristic curves: a nonparametric approach. Int. Biometrics Soc. 227, 20. https://doi.org/10.3847/0067-0049/227/2/20.

Deng, N., Zhang, P., Cieplak, P., Lai, L., 2011. Elucidating the energetics of entropically driven protein–ligand association: calculations of absolute binding free energy and entropy. J. Phys. Chem. B 115, 11902–11910. https://doi.org/10.1021/jp204047b.

Desai, M., Gutman, J., L'Lanziva, A., Otieno, K., Juma, E., Kariuki, S., Ouma, P., Were, V., Laserson, K., Katana, A., Williamson, J., Ter Kuile, F.O, 2015. Intermittent screening and treatment or intermittent preventive treatment with dihydroartemisinin–piperaquine versus intermittent preventive treatment with sulfadoxine–pyrimethamine for the control of malaria during pregnancy in western Kenya: an open-lab. Lancet 386, 2507. https://doi.org/10.1016/S0140-6736(15)00310-4.

Dhorda, M., Amaratunga, C., Dondorp, A.M., 2021. Artemisinin and multidrug-resistant Plasmodium falciparum - a threat for malaria control and elimination. Curr. Opin. Infect. Dis. 34, 432–439. https://doi.org/10.1097/qco.0000000000000766.

Djehoue, R., Adamou, R., Madjid Amoussa, A.O., Medjigbodo, A.A., Laleye, A., Sanni, A., Djogbenou, L.S., Lagnika, L., Mohamed Elshafei Ali, A., 2020. In vitro assessment of antiplasmodial activity and acute oral toxicity of *Dissotis rotundifolia* extracts and fractions on *Plasmodium falciparum* Strains. J. Appl. Life Sci. Int. 23, 8–19. https://doi.org/10.9734/jalsi/2020/v23i530161.

Dondorp, A.M., Von Seidlein, L., 2017. Treatment of uncomplicated *vivax* and *ovale* malaria, in: infectious Diseases, 2-Volume Set. Elsevier 1014–1025. https://doi.org/10.1016/B978-0-7020-6285-8.00117-9 e1.

Dong, Y.W., Liao, M.L., Meng, X.L., Somero, G.N., 2018. Structural flexibility and protein adaptation to temperature: molecular dynamics analysis of malate dehydrogenases of marine molluscs. Proc. Natl. Acad. Sci. USA. 115, 1274–1279. https://doi.org/10.1073/pnas.1718910115.

Egan, W.J., Merz, K.M., Baldwin, J.J., 2000. Prediction of drug absorption using multivariate statistics. J. Med. Chem. 43, 3867–3877. https://doi.org/10.1021/jm000292e.

El Gaaloul, M., Tornesi, B., Lebus, F., Reddy, D., Kaszubska, W., 2022. *Re*-orienting anti-malarial drug development to better serve pregnant women. Malar. J. 21, 1–7. https://doi.org/10.1186/S12936-022-04137-2/FIGURES/1.

Enninful, K.S., Kwofie, S.K., Tetteh-Tsifoanya, M., Lamptey, A.N.L., Djameh, G., Nyarko, S., Ghansah, A., Wilson, M.D., 2022. Targeting the *Plasmodium falciparum*'s thymidylate monophosphate kinase for the identification of novel antimalarial natural compounds. Front. Cell. Infect. Microbiol. 12, 1–13. https://doi.org/10.3389/fcimb.2022.868529.

Fernandes, J., Gattass, C.R., 2009. Topological polar surface area defines substrate transport by multidrug resistance associated protein 1 (MRP1/ABCC1). J. Med. Chem. 52, 1214–1218. https://doi.org/10.1021/jm801389m.

Filimonov, D.A., Lagunin, A.A., Gloriozova, T.A., Rudik, A.V., Druzhilovskii, D.S., Pogodin, P.V., Poroikov, V.V., 2014. Prediction of the biological activity spectra of organic compounds using the pass online web resource. Chem. Heterocycl. Compd. 50, 444–457. https://doi.org/10.1007/s10593-014-1496-1.

Bhat, G., 2022. Medicinal plants and Its pharmacological values. Natural Medicinal Plants. IntechOpen. https://doi.org/10.5772/intechopen.99848.

Ghose, A.K., Viswanadhan, V.N., Wendoloski, J.J., 1999. A knowledge-based approach in designing combinatorial or medicinal chemistry libraries for drug discovery. 1. A qualitative and quantitative characterization of known drug databases. J. Comb. Chem. 1, 55–68. https://doi.org/10.1021/cc9800071.

Goel, R.K., Singh, D., Lagunin, A., Poroikov, V., 2010. PASS-assisted exploration of new therapeutic potential of natural products. Med. Chem. Res. 2010 209 (20), 1509–1514. https://doi.org/10.1007/S00044-010-9398-Y.

Goksuluk, D., Korkmaz, S., Zararsiz, G., Karaagaoglu, A.E., 2016. EasyROC: an interactive web-tool for roc curve analysis using r language environment. R J. 8, 213–230. https://doi.org/10.32614/rj-2016-042.

Gupta, A., Chaudhary, N., Aparoy, P., 2018. MM-PBSA and per-residue decomposition energy studies on 7-Phenyl-imidazoquinolin-4(5H)-one derivatives: identification of crucial site points at microsomal prostaglandin E synthase-1 (mPGES-1) active site. Int. J. Biol. Macromol. 119, 352–359. https://doi.org/10.1016/j.ijbiomac.2018.07.050.

Hadni, H., Bakhouch, M., Elhallaoui, M., 2021. 3D-QSAR, molecular docking, DFT and ADMET studies on quinazoline derivatives to explore novel DHFR inhibitors. J. Biomol. Struct. Dyn. 0, 1–15. https://doi.org/10.1080/07391102.2021.2004233.

Hadni, H., Elhallaoui, M., 2017. Molecular docking and QSAR studies for modeling the antimalarial activity of hybrids 4-anilinoquinoline-triazines derivatives with the wild-type and mutant receptor *pf*-DHFR. https://doi.org/10.1016/j.heliyon.2019.e02357.

Heifets, A., Lilien, R.H., 2010. LigAlign: flexible ligand-based active site alignment and analysis. J. Mol. Graph. Model. 29, 93–101. https://doi.org/10.1016/j.jmgm.2010.05.005.

Heinberg, A., Kirkman, L., 2015. The molecular basis of antifolate resistance in *Plasmodium falciparum*: looking beyond point mutations. Ann. N. Y. Acad. Sci. 1342, 10–18. https://doi.org/10.1111/nyas.12662.

Henriquez, F.L., Williams, D.R.A.M., 2020. Knowing one's enemy: the *Plasmodium* parasite. Antimalar. Agents 49–64. https://doi.org/10.1016/B978-0-08-101210-9.00002-0.

Hyde, J.E., 2005. Exploring the folate pathway in *Plasmodium falciparum*. Acta Trop. https://doi.org/10.1016/j.actatropica.2005.04.002.

Ibraheem, W., Makki, A.A., Alzain, A.A., 2022. Phthalide derivatives as dihydrofolate reductase inhibitors for malaria: molecular docking and molecular dynamics studies. J. Biomol. Struct. Dyn. 0, 1–11. https://doi.org/10.1080/07391102.2022.2080114.

Iwaloye, O., Elekofehinti, O.O., Kikiowo, B., Fadipe, T.M., Akinjiyan, M.O., Ariyo, E.O., Aiyeku, O.O., Adewumi, N.A., 2021. Discovery of traditional chinese medicine derived compounds as wild type and mutant *Plasmodium falciparum* Dihydrofolate Reductase Inhibitors: induced Fit Docking and ADME Studies. Curr. Drug Discov. Technol. 18, 554–569. https://doi.org/10.2174/1570163817999200729122753.

Jiang, Z., You, L., Dou, W., Sun, T., Xu, P., 2019. Effects of an electric field on the conformational transition of the protein: a molecular dynamics simulation study. Polymers (Basel) 11, 1–13. https://doi.org/10.3390/polym11020282.

Kamchonwongpaisan, S., Quarrell, R., Charoensetakul, N., Ponsinet, R., Vilaivan, T., Vanichtanankul, J., Tarnchompoo, B., Sirawaraporn, W., Lowe, G., Yuthavong, Y., 2004. Inhibitors of multiple mutants of *Plasmodium falciparum* dihydrofolate reductase and their antimalarial activities. J. Med. Chem. 47, 673–680. https://doi.org/10.1021/jm030165t.

Kanehisa, M., 2002. The KEGG database. Novartis Found. Symp. 247, 91–101 discussion 101-3, 119–28, 244–52.

Khanna, V., Ranganathan, S., 2009. Physiochemical property space distribution among human metabolites, drugs and toxins. BMC Bioinformatics 10 (Suppl 1), S10. https://doi.org/10.1186/1471-2105-10-S15-S10.

Kumari, R., Kumar, R., Lynn, A., 2014. g_mmpbsa —A GROMACS Tool for high-throughput MM-PBSA calculations. J. Chem. Inf. Model. 54, 1951–1962. https://doi.org/10.1021/ci500020m.

Lagnika, L., Djehoue, R., Yedomonhan, H., Sanni, A., 2016. Ethnobotanical survey of medicinal plants used in malaria management in South Benin. J. Med. Plants Res. 10, 748–756. https://doi.org/10.5897/JMPR2016.6219.

Laskowski, R.A., Swindells, M.B., 2011. LigPlot+: multiple ligand–protein interaction diagrams for drug discovery. J. Chem. Inf. Model. 51, 2778–2786. https://doi.org/10.1021/ci200227u.

Li, Y., Han, L., Liu, Z., Wang, R., 2014. Comparative assessment of scoring functions on an updated benchmark: 2. Evaluation methods and general results. J. Chem. Inf. Model. 54, 1717–1736. https://doi.org/10.1021/ci500081m.

Lobanov, M.Y., Bogatyreva, N.S., Galzitskaya, O.V., 2008. Radius of gyration as an indicator of protein structure compactness. Mol. Biol. 42, 623–628. https://doi.org/10.1134/S0026893308040195.

Manhas, A., Lone, M.Y., Jha, P.C., 2019. Multicomplex-based pharmacophore modeling in conjunction with multi-target docking and molecular dynamics simulations for the identification of PfDHFR inhibitors. J. Biomol. Struct. Dyn. 37, 4181–4199. https://doi.org/10.1080/07391102.2018.1540362.

Mann, A., Egwim, E.C., Banji, B., Abdukadir, N.-.U., Gbate, M., Ekanem, J.T., 2009. Efficacy of *Dissotis rotundifolia* on *Trypanosoma brucei* infection in rats. African J. Biochem. Res. 3, 005–008. https://doi.org/10.5897/AJBR.9000113.

Mharakurwa, S., Kumwenda, T., Mkulama, M.A.P., Musapa, M., Chishimba, S., Shiff, C. J., Sullivan, D.J., Thuma, P.E., Liu, K., Agre, P., 2011. Malaria antifolate resistance with contrasting *Plasmodium falciparum* dihydrofolate reductase (DHFR) polymorphisms in humans and Anopheles mosquitoes. Proc. Natl. Acad. Sci. USA. 108, 18796–18801. https://doi.org/10.1073/pnas.1116162108.

Mohammadi, S., Jafari, B., Asgharian, P., Martorell, M., Sharifi-Rad, J., 2020. Medicinal plants used in the treatment of Malaria: a key emphasis to *Artemisia, Cinchona, Cryptolepis, and Tabebuia genera*. Phyther. Res. 34, 1556–1569. https://doi.org/10.1002/PTR.6628.

Moore, K.A., Simpson, J.A., Scoullar, M.J.L., McGready, R., Fowkes, F.J.I., 2017. Quantification of the association between malaria in pregnancy and stillbirth: a systematic review and meta-analysis. Lancet Glob. Heal. 5, e1101–e1112. https://doi.org/10.1016/s2214-109x(17)30340-6/attachment/6b66cac6-e176-4981-87a1-6d88dd931a97/mmc1.

Muegge, I., Heald, S.L., Brittelli, D., 2001. Simple selection criteria for drug-like chemical matter. J. Med. Chem. 44, 1841–1846. https://doi.org/10.1021/jm015507e.

Mysinger, M.M., Carchia, M., Irwin, J.J., Shoichet, B.K., 2012. Directory of useful decoys, enhanced (DUD-E): better ligands and decoys for better benchmarking. J. Med. Chem. 55, 6582–6594. https://doi.org/10.1021/jm300687e.

Nelson, F.R.S., Hoosseintehrani, B., 1982. Effects of benzylphenol and benzyl-1,3-benzodioxole derivatives on fertility and longevity of the yellow fever mosquito (Diptera: culicidae). J. Econ. Entomol. 75, 877–878. https://doi.org/10.1093/jee/75.5.877.

O'Boyle, N.M., Banck, M., James, C.A., Morley, C., Vandermeersch, T., Hutchison, G.R., 2011. Open Babel: an open chemical toolbox. J. Cheminform. 3, 33. https://doi.org/10.1186/1758-2946-3-33.

Pantsar, T., Poso, A., 2018. Binding affinity via docking: fact and Fiction. Molecules 23. https://doi.org/10.3390/molecules23081899.

Parasuraman, S., 2011. Toxicological screening. J. Pharmacol. Pharmacother. 2, 74–79. https://doi.org/10.4103/0976-500X.81895.

Pence, H.E., Williams, A., 2010. ChemSpider: an online chemical information resou rce. J. Chem. Educ. 87, 1123–1124. https://doi.org/10.1021/ed100697w.

R Core, 2020. R: a language and environment for statistical computing. R Foundation for Statistical Computing, Vienna, Austria.

Raschka, S., 2017. Molecular docking, estimating free energies of binding, and AutoDock ' s semi-empirical force field Introduction molecular docking 1–19.

Rath, G., Touré, A., Nianga, M., Wolfender, J.L., Hostettmann, K., 2014. Characterization of C-glycosylflavones from *Dissotis rotundifolia* by liquid chromatography — UV diode array detection — Tandem mass spectrometry. Chromatogr 415 (41), 332–342. https://doi.org/10.1007/BF02688048, 1995.

Rothwell, J.A., Perez-Jimenez, J., Neveu, V., Medina-Remon, A., M'Hiri, N., Garcia-Lobato, P., Manach, C., Knox, C., Eisner, R., Wishart, D.S., Scalbert, A., 2013. Phenol-Explorer 3.0: a major update of the phenol-explorer database to incorporate data on the effects of food processing on polyphenol content. Database 2013, bat070–bat070. https://doi.org/10.1093/database/bat070.

Sander, T., Freyss, J., Von Korff, M., Rufener, C., 2015. DataWarrior: an open-source program for chemistry aware data visualization and analysis. J. Chem. Inf. Model. 55, 460–473. https://doi.org/10.1021/ci500588j.

Shamshad, H., Bakri, R., Mirza, A.Z., 2022. Dihydrofolate reductase, thymidylate synthase, and serine hydroxy methyltransferase: successful targets against some infectious diseases. Mol. Biol. Reports 497 (49), 6659–6691. https://doi.org/10.1007/S11033-022-07266-8, 2022.

Shukla, V., Singh, P., kumar, D., Konwar, R., Singh, B., Kumar, B., 2021. Phytochemical analysis of high value medicinal plant *Valeriana jatamansi* using LC-MS and it's in-vitro anti-proliferative screening. Phytomedicine Plus 1, 100025. https://doi.org/10.1016/J.PHYPLU.2021.100025.

Singh, I.V., Mishra, S., 2018. Molecular docking analysis of pyrimethamine derivatives with *Plasmodium falciparum* dihydrofolate reductase. Bioinformation 14, 232–235. https://doi.org/10.6026/97320630014232.

Sinha, S., Wang, S.M., 2020. Classification of VUS and unclassified variants in BRCA1 BRCT repeats by molecular dynamics simulation. Comput. Struct. Biotechnol. J. 18, 723–736. https://doi.org/10.1016/j.csbj.2020.03.013.

Stank, A., Kokh, D.B., Fuller, J.C., Wade, R.C., 2016. Protein binding pocket dynamics. Acc. Chem. Res. 49, 809–815. https://doi.org/10.1021/acs.accounts.5b00516.

Stanzione, F., Giangreco, I., Cole, J.C., 2021. Use of Molecular Docking Computational Tools in Drug discovery, 1st ed, Progress in Medicinal Chemistry. Elsevier B.V. https://doi.org/10.1016/bs.pmch.2021.01.004.

Sunghwan, K., Chen, J., Cheng, T., Gindulyte, A., He, J., He, S., Li, Q., Shoemaker, B.A., Thiessen, P.A., Yu, B., Zaslavsky, L., Zhang, J., Bolton, E.E., 2021. PubChem in 2021: new data content and improved web interfaces. Nucleic Acids Res 49, D1388–D1395. https://doi.org/10.1093/nar/gkaa971.

Tian, W., Chen, C., Lei, X., Zhao, J., Liang, J., 2018. CASTp 3.0: computed atlas of surface topography of proteins. Nucleic Acids Res 46, W363–W367. https://doi.org/10.1093/nar/gky473.

Trott, O., Olson, A.J., 2009. AutoDock Vina: improving the speed and accuracy of docking with a new scoring function, efficient optimization, and multithreading. J. Comput. Chem. 31 https://doi.org/10.1002/jcc.21334. NA-NA.

Uzor, P.F., Prasasty, V.D., Agubata, C.O., 2020. Natural products as sources of antimalarial drugs. evidence-based complement. Altern. Med. https://doi.org/10.1155/2020/9385125, 2020.

Veber, D.F., Johnson, S.R., Cheng, H.-Y., Smith, B.R., Ward, K.W., Kopple, K.D., 2002. Molecular properties that influence the oral bioavailability of drug candidates. J. Med. Chem. 45, 2615–2623. https://doi.org/10.1021/jm020017n.

Waller, D.G., Sampson, A.P., 2018. Chemotherapy of infections. Med. Pharmacol. Ther. 581–629. https://doi.org/10.1016/B978-0-7020-7167-6.00051-8.

Wang, C., Nguyen, P.H., Pham, K., Huynh, D., Le, T.N., Wang, H., Ren, P., Luo, R., 2017. Calculating protein-ligand binding affinities with MMPBSA: method and error analysis 37, 2436–2446. https://doi.org/10.1002/jcc.24467.

WHO, 2021. Word Malaria Report 2021, Word malaria report Geneva: world Health Organization. (2021).

Xu, Y., Capistrano, R., Dhooghe, L., Foubert, K., Lemière, F., Maregesi, S., Baldé, A., Apers, S., Pieters, L., 2011. Herbal medicines and infectious diseases: characterization by LC-SPE-NMR of some medicinal plant extracts used against malaria. Planta Med 77, 1139–1148. https://doi.org/10.1055/s-0030-1270719.

Yeboah, O., Osafo, N., 2017. Review of the ethno-medical, phytochemical, pharmacological and toxicological studies on *Dissotis rotundifolia* (Sm.) Triana. J. Complement. Altern. Med. Res. 2, 1–11. https://doi.org/10.9734/JOCAMR/2017/32212.

Yinnon, A., Theanacho, E., Grady, R., Spira, D., Hershko, C., 1989. Antimalarial effect of HBED and other phenolic and catecholic iron chelators. Blood 74, 2166–2171. https://doi.org/10.1182/blood.V74.6.2166.2166.

Yuan, S., Chan, H.C.S., Hu, Z., 2017. Using PyMOL as a platform for computational drug design. Wiley Interdiscip. Rev. Comput. Mol. Sci. 7 https://doi.org/10.1002/wcms.1298.

Yuvaniyama, J., Chitnumsub, P., Kamchonwongpaisan, S., Vanichtanankul, J., Sirawaraporn, W., Taylor, P., Walkinshaw, M.D., Yuthavong, Y., 2003. Insights into antifolate resistance from malarial DHFR-TS structures. Nat. Struct. Biol. 10, 357–365. https://doi.org/10.1038/nsb921.

Zoete, V., Cuendet, M.A., Grosdidier, A., Michielin, O., 2011. SwissParam: a fast force field generation tool for small organic molecules. J. Comput. Chem. 32, 2359–2368. https://doi.org/10.1002/jcc.21816.